LETTER

doi:10.1038/nature12131

Atmospheric confinement of jet streams on Uranus and Neptune

Yohai Kaspi[1], Adam P. Showman[2], William B. Hubbard[2], Oded Aharonson[1,3] & Ravit Helled[4]

The observed cloud-level atmospheric circulation on the outer planets of the Solar System is dominated by strong east–west jet streams. The depth of these winds is a crucial unknown in constraining their overall dynamics, energetics and internal structures. There are two approaches to explaining the existence of these strong winds. The first suggests that the jets are driven by shallow atmospheric processes near the surface[1–3], whereas the second suggests that the atmospheric dynamics extend deeply into the planetary interiors[4,5]. Here we report that on Uranus and Neptune the depth of the atmospheric dynamics can be revealed by the planets' respective gravity fields. We show that the measured fourth-order gravity harmonic, J_4, constrains the dynamics to the outermost 0.15 per cent of the total mass of Uranus and the outermost 0.2 per cent of the total mass of Neptune. This provides a stronger limit to the depth of the dynamical atmosphere than previously suggested[6], and shows that the dynamics are confined to a thin weather layer no more than about 1,000 kilometres deep on both planets.

Measurable perturbations to the gravity fields of Uranus and Neptune can result from mass anomalies due to two sources—the rapid rotation of these planets, which distorts the planets into a non-spherical (oblate) shape, and density perturbations, which result from fast atmospheric winds[6–10] organized on both planets into a broad zone of westward flow near the equator and eastward flow at high latitudes (Fig. 1). The gravity field can be decomposed into spherical gravity harmonics, (J_n), which are defined as a weighted integral over the planets' density distribution, $J_n = -(Ma^n)^{-1}\int P_n \rho r^n \mathrm{d}^3\boldsymbol{r}$, where P_n is the nth Legendre polynomial, M is the planetary mass, a is the mean planetary radius, ρ is the local density and r is the local radius[11]. On planets with internal dynamics (winds), the density is perturbed by the flow so that the total density in J_n can be written as $\rho = \rho_{\mathrm{static}} + \rho'$, where the density ρ_{static} is the hydrostatic density, and ρ' are the density fluctuations arising from internal dynamics. The gravity harmonics, can be then similarly decomposed into two parts $J_n = J_n^{\mathrm{static}} + \Delta J_n^{\mathrm{dyn}}$, where the first part ($J_n^{\mathrm{static}}$) is due to the oblateness and radial density distribution of the planet and the second part ($\Delta J_n^{\mathrm{dyn}}$) is due to the dynamical perturbations arising from winds[8,10].

In order to place an upper bound on the depth of the atmospheric circulation on Uranus and Neptune, we determine the difference between the observed J_4 and J_4^{static} resulting from wind-free models set to match all other observational constraints besides J_4. Any difference in these quantities places constraints on the meteorological contribution to J_4. Of course, the observed J_4 has uncertainties; moreover, there exists a full family of interior models ρ_{static} with different J_4^{static} values. Therefore, this difference can take on a wide range of possible values. Here we determine the maximum possible difference, which then determines the maximum possible contribution that dynamics can make to J_4.

To determine the widest possible range of J_4^{static} values, we compute an ensemble of interior density profiles, $\rho_{\mathrm{static}}(r)$, for each planet, calculated using the theory of figures[12], to third order, constrained to match the total mass, J_2, mean radius, and the atmospheric density and its derivative at a pressure level of 1 bar (see Supplementary Information). The resulting range of J_4^{static} values lie between -32.5×10^{-6} and -30.5×10^{-6} for Uranus, and between -34.5×10^{-6} and -31×10^{-6} for Neptune (Fig. 2 and Supplementary Fig. 1). Thus, even without constraining the interior models to the observed J_4 (for example, ref. 13), knowledge of the observed J_2 is enough to limit the possible solutions to be close to the observed J_4 values of $(-30.44\pm1.02)\times10^{-6}$ and $(-33.40\pm2.90)\times10^{-6}$ for Uranus and Neptune, respectively[14,15]. Results from models using more sophisticated equations of state[6,16–19] are within the same range for both planets. On the basis of the J_4^{static} values from the ensemble of interior models (Fig. 2 and Supplementary Fig. 1), and the observed values of J_4 (J_4^{observed}) including their uncertainties[14,15], and assuming $\Delta J_4^{\mathrm{dyn}} = J_4^{\mathrm{observed}} - J_4^{\mathrm{static}}$, we find that $\Delta J_4^{\mathrm{dyn}}$ must be within the range $-1\times10^{-6} < \Delta J_4^{\mathrm{dyn}} < 3\times10^{-6}$ for Uranus, and $-5\times10^{-6} < \Delta J_4^{\mathrm{dyn}} < 4\times10^{-6}$ for Neptune.

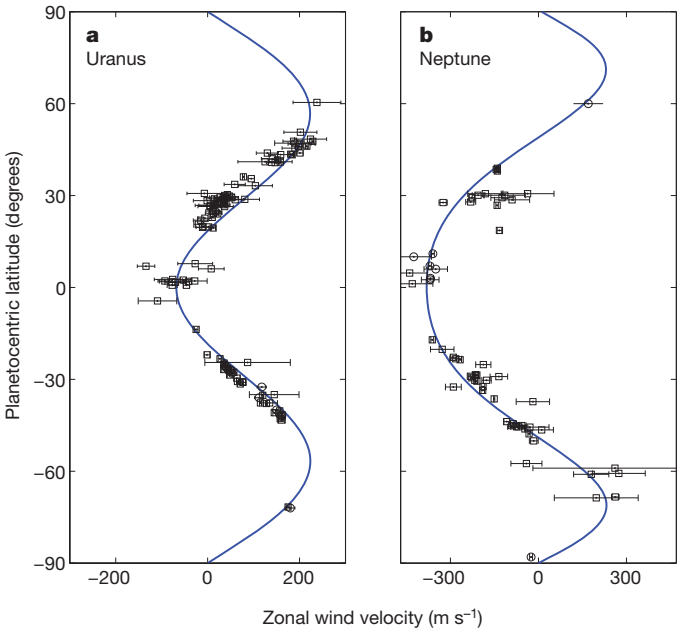

Figure 1 | Observed cloud-level zonally averaged zonal winds on Uranus and Neptune. **a**, Observations of Uranus from Voyager 2 (circles) and from HST measurements (squares)[27,28]. The solid line is an empirical fit to the data[28]. **b**, Observations of Neptune from Voyager 2 (circles)[29] and from HST measurements (squares)[30]. The solid line is an empirical fit to the data[29], constrained to zero at the poles. The cloud-level atmospheric circulations on Uranus and Neptune have a generally similar structure, despite the differences in solar insolation (Uranus has an obliquity of 98°, whereas that of Neptune is 29°), and internal heating (Neptune's internal/solar heating ratio is roughly1.6, whereas that of Uranus is only 0.06). Error bars represent cloud tracking and navigational errors[27–30].

[1]Department for Environmental Sciences and Center for Planetary Science, Weizmann Institute of Science, Rehovot 76100, Israel. [2]Lunar and Planetary Laboratory, University of Arizona, Tucson, Arizona 85721, USA. [3]Department of Geological and Planetary Sciences, California Institute of Technology, Pasadena, California 91125, USA. [4]Department of Geophysics and Planetary Science, Tel Aviv University, Tel Aviv 69978, Israel.

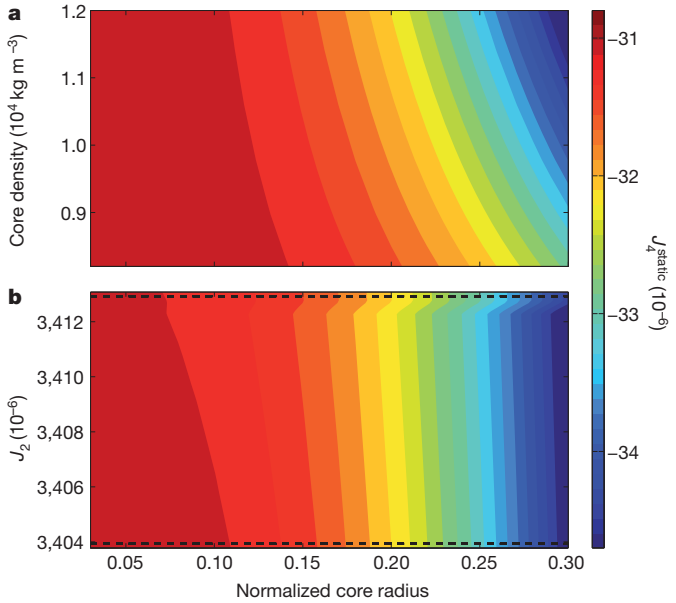

Figure 2 | J_4^{static} over a wide range of interior models for Neptune. **a**, J_4^{static} as a function of normalized core radius and core density, with J_2 held constant at the mean observed value[15] of $J_2 = 3{,}408.4 \times 10^{-6}$. **b**, J_4^{static} as a function of normalized core radius and J_2, with the core density set to 1.01×10^4 kg m^{-3}, and $J_2 = (3{,}408.4 \pm 4.5) \times 10^{-6}$ varying between the observed uncertainties (dashed lines). We specifically do not constrain the solution to J_4, because we are interested in the possible range of J_4^{static} given the other constraints. We allow the constant-density core to extend up to 30% of the planet's radius (Fig. 3), its density to be up to 1.2×10^4 kg m^{-3} (refs 16, 17, 19) and J_2 to vary within the observed error estimates (see further details in Supplementary Information). A similar figure for Uranus appears as Supplementary Fig. 1.

Understanding the dynamical implications of these inferred ΔJ_4^{dyn} limit values requires knowledge of the zonal velocity structure. Because the planets are rapidly rotating, and Coriolis accelerations are dominant over inertial accelerations (small Rossby number), surfaces of constant angular momentum per unit mass will be nearly parallel to the axis of rotation[20,21]. To leading order, this results in no interior flow crossing surfaces of constant angular momentum[3,20,21], and thus the fluid motion can be only along cylinders parallel to the spin axis, although the zonal wind velocity can decay towards the high-pressure interior[20,22]. We therefore assume that the zonal wind field has the general form $u(r, \theta) = u_0 \exp[(r - a)/H]$ where $u_0(r,\theta)$ is the observed northern and southern hemisphere average cloud level zonal wind (Fig. 1) extended constantly along the direction of the axis of rotation (θ is latitude), and H is an e-folding decay depth of the cloud-level winds representing the possible shear of the winds[8,10]. H is a free parameter, and varying it systematically allows exploration of the dependence of the gravity harmonics on the vertical extent of the winds. Thus, when $H \gg a$ the zonal wind is nearly constant along the direction of the axis of rotation, and as H is decreased the zonal velocity decreases more rapidly with depth[8,10]. Because the dynamics are in the regime of small Rossby numbers, the flow to leading order is in geostrophic balance[23], and therefore the thermal wind balance must hold so that

$$(2\Omega \cdot \nabla)[\rho_{static} \boldsymbol{u}] = \nabla \rho' \times \boldsymbol{g}_0, \quad (1)$$

where Ω is the planetary rotation rate, $\boldsymbol{u}(\boldsymbol{r})$ is the full three-dimensional velocity and $\boldsymbol{g_0}(\boldsymbol{r})$ is the mean gravity vector[20,23]. Here the thermal wind balance is written in a general form without making any assumptions about the depth of the circulation[20]. Because the dynamics are a perturbation to the mean hydrostatic state, and the planets' deviation from spherical geometry is small (the equatorial radius is larger than the polar radius by 2.3% and 1.7% for Uranus and Neptune, respectively), we calculate the dynamical contribution to the gravity harmonics (ΔJ_n^{dyn}) in spherical geometry. Thus, given the hydrostatic density $\rho_{static}(r)$ from interior models (for example, Fig. 3), the mean gravity $\boldsymbol{g_0}$ (which is calculated by integrating ρ_{static} radially) and the zonal velocity $u(r,\theta)$, the dynamical perturbation density $\rho'(r,\theta)$ can be calculated from the zonal component of equation (1), and will depend on the decay parameter H and an integration constant $\rho'_0(r)$. This integration constant has no contribution to ΔJ_n^{dyn} under spherical geometry, and has a negligible contribution in an oblate spheroid because $\rho'_0 \ll \rho_{static}$ (see Supplementary Information).

Comparing the allowable range of ΔJ_4^{dyn} inferred from $J_4^{observed} - J_4^{static}$ (dashed red lines in Fig. 4) to ΔJ_4^{dyn} calculated by the dynamical model with different wind depths allows placing an upper limit on the depth of the zonal winds. These values are calculated by systematically varying the decay depth H between 10 km and 10^5 km (thus from very shallow winds, to winds nearly penetrating the depth of the planet), calculating the resulting density perturbations (equation (1)) and then calculating ΔJ_4^{dyn} by integration over the spherical domain. We repeated this analysis for all models in our ensemble of interior models for $\rho_{static}(r)$, as well as for interior models of $\rho_{static}(r)$ inferred from more complex equations of state[6,16,19]. All solutions lie between the blue curves in Fig. 4 for each of the planets.

Therefore, the largest possible depth of the flow where $\Delta J_4^{dyn} = 4 \times 10^{-6}$ for Neptune and $\Delta J_4^{dyn} = 3 \times 10^{-6}$ for Uranus occurs for shallow depths of roughly $H = 1{,}100$ km for both planets (Fig. 4). This means that the depth of the circulation on Neptune cannot exceed a pressure level of roughly 4,000 bar, which corresponds to the uppermost 0.2% of the total mass of the planet. Owing to the weaker winds on Uranus, the effect of the dynamics on ΔJ_4^{dyn} is smaller; however, because the planet is less massive the upper limit on the core size is lower (Supplementary Fig. 1), and therefore the maximum possible depth in Fig. 4 is similar to that of Neptune and corresponds to ~2,000 bar (which is roughly the outermost 0.15% of the planetary mass).

Previous studies using potential theory[6] have shown that full differential rotation along cylinders is impossible for Neptune because the resulting J_4 will be large and positive ($\sim 10^{-4}$), whereas the observed value is negative. In the limit of deep winds (large H), our results for ΔJ_4^{dyn} match those results (Fig. 4). Here however, by using a continuous range of zonal velocity decay depths, and using today's better known observed

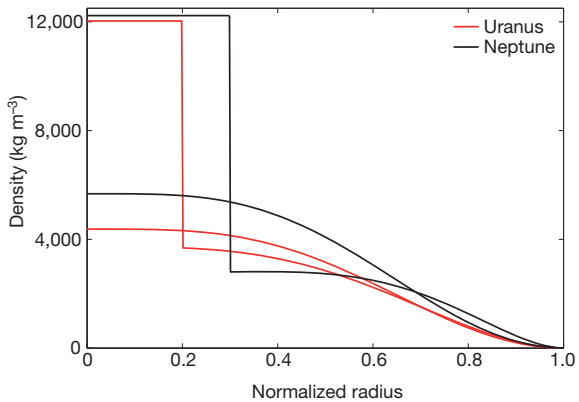

Figure 3 | Radial density profiles for two different interior models of Uranus and Neptune. Interior profiles shown are the extreme cases of $\rho_{static}(r)$ from our suite of interior models. For each planet, we show here one model that has a constant core density of $\sim 1.2 \times 10^4$ kg m^{-3} reaching 30% of the planet's radius on Neptune (black) and 20% of the planet's radius on Uranus (red), and another model that does not have a constant density core. We used a suite of more than 3,000 profiles for Neptune and more than 1,500 profiles for Uranus, which are between these two extreme cases. All cases are constrained to match the planets' mass, J_2, mean radius, and the atmospheric density and its derivative at 1 bar, but are not constrained to the observed J_4 (see Supplementary Information). Density profiles based on three-layer models[6,16,19] were also used.

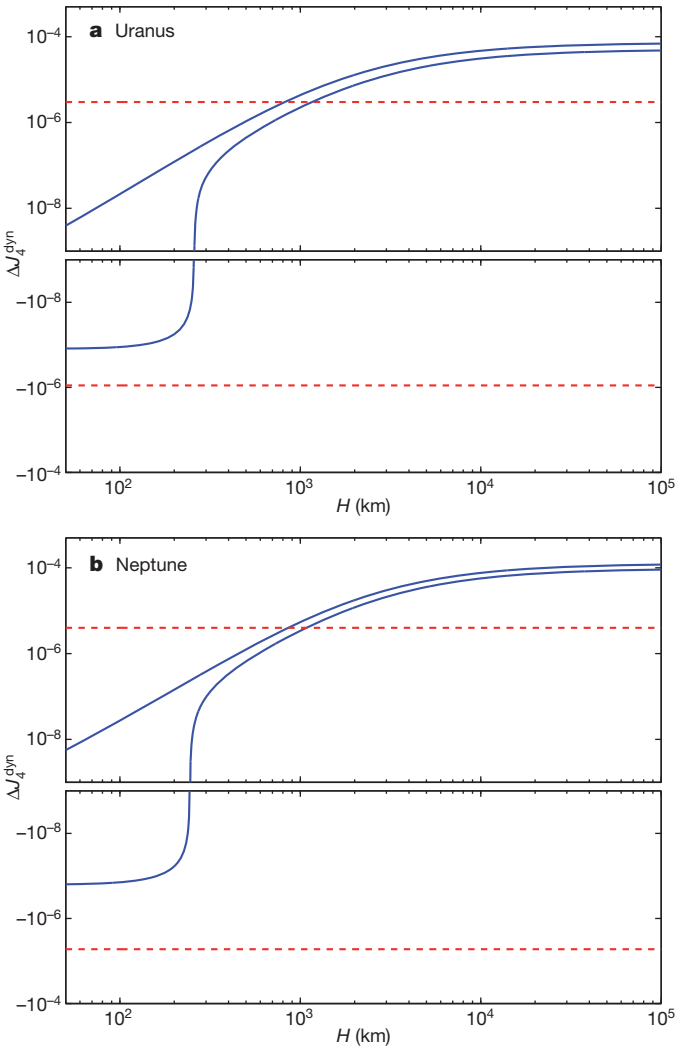

Figure 4 | ΔJ_4^{dyn} as function of the decay height H for Uranus and Neptune. **a**, Uranus; **b**, Neptune. All possible solutions for the range of interior models explored in this study are between the two blue lines for each planet. The dashed lines are the maximum and minimum possible values for ΔJ_4^{dyn} calculated as the difference between the observed J_4 and J_4^{static} obtained from the interior models (Fig. 2 and Supplementary Fig. 1). Only solutions within the two dashed red lines are possible solutions for the dynamical contribution to J_4, and therefore H must be limited to less than ~1,100 km for both Uranus and Neptune. On Uranus, this depth corresponds to a pressure of roughly 2,000 bar or the outermost 0.15% of the mass. For Neptune, this is equivalent to a pressure of roughly 4,000 bar or the outermost 0.2% of the mass. For lower values of H (not shown), all ΔJ_4^{dyn} values converge to zero. For each planet, the bottom half of the plot is the negative of the log-scale to reflect the negative numbers on a log-scale.

values of J_4 (refs 14, 15), we provide much stronger constraints on the depth of the flow: we constrain the dynamics to the top few thousand bars, instead of the top few hundred thousand bars[6].

The confinement of the strong jets on Uranus and Neptune to a shallow weather layer implies that the dynamics controlling zonal jets are likely to come from shallow processes, rather than from deep columnar structures that penetrate through the planet. Nevertheless, internal heat may be significant in driving these jets, particularly on Neptune where the internal heat flux is 1.6 times stronger than the heating from the Sun[24]. Decay of the fast surface winds to small values within a shallow layer requires large horizontal density contrasts on isobars in the deep atmosphere. These could plausibly be provided by latent heating due to condensation of water at pressures of ~300 bar (ref. 2).

It is important to note that our results are an upper limit to the depth of the dynamics, owing to the conservative approach taken here of using the widest range of reasonable interior models. These upper limits also hold when repeating the analysis with state-of-the-art three-layer interior structure models consisting of large ice/rock-rich cores[19]. Further understanding of the interior structures will probably narrow the range of possible J_4^{static} values, and thus confine the dynamics to be even shallower, although the precise constraint can depend on the details of the equation of state and density structure assumed. It is possible to imagine more complex dynamical scenarios (for example, where the depth of the winds varies in latitude). ΔJ_4^{dyn} is sensitive to the long-wavelength component of such variation, and, for this component, our results are robust and not model-dependent. In particular, the latitudinally averaged H must be smaller than the limits described in Fig. 4. We find these results to be robust to within a few per cent even when considering uncertainty in the exact rotation period[25,26]. Although current knowledge of the gravity fields of Jupiter and Saturn is not sufficiently precise for a similar analysis, expected observations from the low-flying Juno and Cassini orbiters will enable tighter constraints on their low-order gravity fields, and hence on the depth of their dynamics[8,10].

Received 4 October 2012; accepted 22 March 2013.

1. Read, P. L. Clearer circulation on Uranus. *Nature* **325,** 197–198 (1987).
2. Lian, Y. & Showman, A. P. Generation of equatorial jets by large-scale latent heating on the giant planets. *Icarus* **207,** 373–393 (2010).
3. Liu, J. & Schneider, T. Mechanisms of jet formation on the giant planets. *J. Atmos. Sci.* **67,** 3652–3672 (2010).
4. Suomi, V. E., Limaye, S. S. & Johnson, D. R. High winds of Neptune — a possible mechanism. *Science* **251,** 929–932 (1991).
5. Aurnou, J., Heimpel, M. & Wicht, J. The effects of vigorous mixing in a convective model of zonal flow on the ice giants. *Icarus* **190,** 110–126 (2007).
6. Hubbard, W. B. *et al.* Interior structure of Neptune — comparison with Uranus. *Science* **253,** 648–651 (1991).
7. Hubbard, W. B. Gravitational signature of Jupiter's deep zonal flows. *Icarus* **137,** 357–359 (1999).
8. Kaspi, Y., Hubbard, W. B., Showman, A. P. & Flierl, G. R. Gravitational signature of Jupiter's internal dynamics. *Geophys. Res. Lett.* **37,** L01204 (2010).
9. Kong, D., Zhang, K. & Schubert, G. On the variation of zonal gravity coefficients of a giant planet caused by its deep zonal flows. *Astrophys. J.* **748,** 143 (2012).
10. Kaspi, Y. Inferring the depth of the zonal jets on Jupiter and Saturn from odd gravity harmonics. *Geophys. Res. Lett.* **40,** 676–680 (2013).
11. Hubbard, W. B. *Planetary Interiors* (Van Nostrand Reinhold, 1984).
12. Zharkov, V. N. & Trubitsyn, V. P. *Physics of Planetary Interiors* (Pachart Publishing House, 1978).
13. Helled, R., Anderson, J. D., Podolak, M. & Schubert, G. Interior models of Uranus and Neptune. *Astrophys. J.* **726,** 15 (2011).
14. Jacobson, R. A. The gravity field of the Uranian system and the orbits of the Uranian satellites and rings. *Bull. Am. Astron. Soc.* **39 (3),** 453–453 (2007).
15. Jacobson, R. A. The orbits of the Neptunian satellites and the orientation of the pole of Neptune. *Astrophys. J.* **137,** 4322–4329 (2009).
16. Hubbard, W. B. & Marley, M. S. Optimized Jupiter, Saturn, and Uranus interior models. *Icarus* **78,** 102–118 (1989).
17. Podolak, M., Weizman, A. & Marley, M. Comparative models of Uranus and Neptune. *Planet. Space Sci.* **43,** 1517–1522 (1995).
18. Fortney, J. J. & Nettelmann, N. The interior structure, composition, and evolution of giant planets. *Space Sci. Rev.* **152,** 423–447 (2010).
19. Nettelmann, N., Helled, R., Fortney, J. J. & Redmer, R. New indication for a dichotomy in the interior structure of Uranus and Neptune from the application of modified shape and rotation data. *Planet. Space Sci.* **77,** 143–151 (2013).
20. Kaspi, Y., Flierl, G. R. & Showman, A. P. The deep wind structure of the giant planets: results from an anelastic general circulation model. *Icarus* **202,** 525–542 (2009).
21. Schneider, T. & Liu, J. Formation of jets and equatorial superrotation on Jupiter. *J. Atmos. Sci.* **66,** 579–601 (2009).
22. Liu, J., Goldreich, P. M. & Stevenson, D. J. Constraints on deep-seated zonal winds inside Jupiter and Saturn. *Icarus* **196,** 653–664 (2008).
23. Pedlosky, J. *Geophysical Fluid Dynamics* (Spinger, 1987).
24. Pearl, J. C. & Conrath, B. J. The albedo, effective temperature, and energy balance of Neptune, as determined from Voyager data. *J. Geophys. Res.* **96,** 18921–18930 (1991).
25. Helled, R., Anderson, J. D. & Schubert, G. Uranus and Neptune: shape and rotation. *Icarus* **210,** 446–454 (2010).
26. Karkoschka, E. Neptune's rotational period suggested by the extraordinary stability of two features. *Icarus* **215,** 439–448 (2011).
27. Hammel, H. B., de Pater, I., Gibbard, S., Lockwood, G. W. & Rages, K. Uranus in 2003: zonal winds, banded structure, and discrete features. *Icarus* **175,** 534–545 (2005).
28. Sromovsky, L. A. & Fry, P. M. Dynamics of cloud features on Uranus. *Icarus* **179,** 459–484 (2005).

29. Sromovsky, L. A., Limaye, S. S. & Fry, P. M. Dynamics of Neptune's major cloud features. *Icarus* **105,** 110–141 (1993).
30. Sromovsky, L. A., Fry, P. M., Dowling, T. E., Baines, K. H. & Limaye, S. S. Neptune's atmospheric circulation and cloud morphology: changes revealed by 1998 HST imaging. *Icarus* **150,** 244–260 (2001).

Supplementary Information is available in the online version of the paper.

Acknowledgements Y.K. and O.A. thank the Helen Kimmel Center for Planetary Science at the Weizmann Institute of Science for support. A.P.S. and W.B.H. acknowledge support by NASA.

Author Contributions Y.K. and A.P.S. initiated and designed the research. Y.K. performed the dynamical gravity harmonics calculations and wrote the paper. R.H. performed the static interior model calculations and their interpretation. All authors contributed to the discussion of the results.

Author Information Reprints and permissions information is available at www.nature.com/reprints. The authors declare no competing financial interests. Readers are welcome to comment on the online version of the paper. Correspondence and requests for materials should be addressed to Y.K. (yohai.kaspi@weizmann.ac.il).